Supplemental Material

Supplemental Methods

Histopathological analysis. H&E liver sections were analyzed by 2 experienced liver pathologists (Frank Dombrowski and Matthias Evert) based on the criteria by Frith and Ward (1). Cholangiomas (synonymous with biliary adenomas and cholangiocellular adenomas) are benign cholangiocellular lesions that compress the surrounding parenchyma, but lack cytological atypia, substantial mitotic/apoptotic activity, necrosis, infiltration/invasion, or fibrosis. Cholangiomas can be cystic and are then referred to as cystic cholangiomas or cystadenomas. Cholangiocellular lesions that show cytological atypia and substantial proliferation are defined as intracystic papillary neoplasms with intraepithelial neoplasia by the most recent WHO guidelines. If these neoplasms are the result of malignant transformation of benign cystadenomas they are commonly referred to as cystadenocarcinomas. Cystadenocarcinomas that invade the surrounding liver tissue resemble cholangiocarcinomas (CCs). CCs are characterized by the presence of atypical tumor cells that form ductules, glands or solid sheets, and by clear local or vascular invasion and the potential for metastasis. In the absence of these features, the diagnosis of CC requires the presence of severe cytological atypia (nuclear pleomorphism, prominent nucleoli, basophilic cytoplasm, nuclear hyperchromasia or high nuclear/cytoplasmic ratio), substantial mitotic/apoptotic activity, necrosis, and desmoplastic stromal reaction or fibrosis.

Immunostaining of frozen sections. Liver tissue was embedded in optimum cutting temperature compound (Tissue-Tek, Sakura Finetek) and frozen on dry ice in cold 2-Methylbutane. Frozen sections were cut at 5 µm, blocked with 5% goat serum, labeled

with primary antibodies overnight at 4°C and secondary antibody for 30 minutes at room temperature (Supplemental Tables 1 and 2). Nuclear DNA was stained with 300 nM Dapi (Millipore).

Immunostaining of paraffin sections. Liver tissue was fixed in 4% paraformaldehyde overnight at 4°C, washed in 75% ethanol overnight at 4°C and embedded in paraffin. Slides were dewaxed with xylene and rehydrated through a series of washes with incrementally decreasing percentages of ethanol. Antigen retrieval was performed in 10 mM sodium citrate buffer (pH 6.0) by placement in a microwave on high for 10 minutes, followed by cooling down for 20 minutes at room temperature. After blocking with 5% goat serum and the Avidin/Biotin Blocking Kit (Vector Laboratories), slides were incubated with primary antibody overnight at 4°C (Supplemental Table 1). Slides were then treated with 3% hydrogen peroxide for 10 minutes to inhibit endogenous peroxidase activity. Detection was performed with the Elite ABC Kit (Vector Laboratories) and DAB Substrate (Dako).

Electron microscopy. Liver specimens of 1-2 mm^3 were cut with a razor blade, fixed in 2.5% glutaraldehyde (Sigma-Aldrich), postfixed with osmium tetroxide, embedded in glycid ether 100 (both Carl Roth), and cut with the diamond knife of an Leica Ultracut UCT ultramicrotome. Ultrathin sections of 70-90 nm were stained with uranyl acetate and lead citrate (both Sigma-Aldrich) according to standard protocols (2), and examined with a Zeiss Libra 120 electron microscope. Periodic acid-Schiff (PAS) staining was used to identify hepatocytes with low glycogen content.

qRT-PCR. Total RNA was extracted from frozen liver samples using Trizol (Invitrogen) and digested with DNase I (Ambion) to eliminate contamination with genomic DNA. Reverse transcription and qRT-PCR were performed using qScript cDNA Supermix (Quanta Biosciences) and SYBR Green (ABI), respectively. 18S rRNA was used as an internal control. Primer sequences were: CGGCTACCACATCCAAGGAA (forward), GCTGGAATTACCGCGGCT (reverse) for 18S; TCTGCTGGCACGCAAGAAG (forward), TCGGCAGGTTCTGGAAACTG (reverse) for *Afp*; GCGGCTCAGAGAGACTGTG (forward), CCAAGCATTTAGACGCCAGTTT (reverse) for *Epcam*.

qPCR. Genomic DNA was extracted with the QiAamp DNA Mini Kit (Qiagen) and incubated with RNase A to eliminate RNA. qPCR was performed on 75 ng DNA using SYBR Green in a ViiA 7 system (both Applied Biosystems). *Gapdh* was used as internal control. Primer sequences were: TGTTGAAGTCACAGGAGACAACCT (forward), AACCTGCCAAGTATGATG ACATCA (reverse) for *Gapdh*; TTTCCCGCAGAACCTGAAGATG (forward), ATCCGCCGCATAACCAGTG (reverse) for *Cre*.

Immunoblotting. Frozen liver samples were homogenized in lysis buffer [30 mM Tris (pH 7.5), 150 mM NaCl, 1% NP-40, 0.5% Na-deoxycholate, 0.1% SDS, 10% glycerol, and 2 mM EDTA] containing the Complete Protease Inhibitor Cocktail (Roche Molecular Biochemicals) and sonicated. Protein concentrations were determined with the Bio-Rad Protein Assay Kit using bovine serum albumin as a standard. Aliquots of 100 μg were

denatured by boiling in Tris-Glycine SDS Sample Buffer (Invitrogen), separated by SDS-PAGE, and transferred onto nitrocellulose membranes (Invitrogen) by electroblotting. Membranes were blocked in 5% non-fat dry milk in Tris-buffered saline containing 0.1% Tween 20 for 1 hour and probed with primary antibody overnight, followed by incubation with horseradish peroxidase (HRP)-secondary antibody for 1 hour and visualization with SuperSignal West Pico Chemiluminescent Substrate (Pierce) (Supplemental Tables 1 and 2).

2/3 PH. With mice under isofluorane anesthesia and sterile conditions, 2/3 of the liver were surgically removed as previously described (3).

Supplemental References

1. Frith, C.H., Ward, J.M., and Turusov, V.S. 1994. Tumours of the liver. *IARC Sci Publ*:223-269.
2. Richardson, K.C., Jarett, L., and Finke, E.H. 1960. Embedding in epoxy resins for ultrathin sectioning in electron microscopy. *Stain Technol* 35:313-323.
3. Mitchell, C., and Willenbring, H. 2008. A reproducible and well-tolerated method for 2/3 partial hepatectomy in mice. *Nat Protoc* 3:1167-1170.

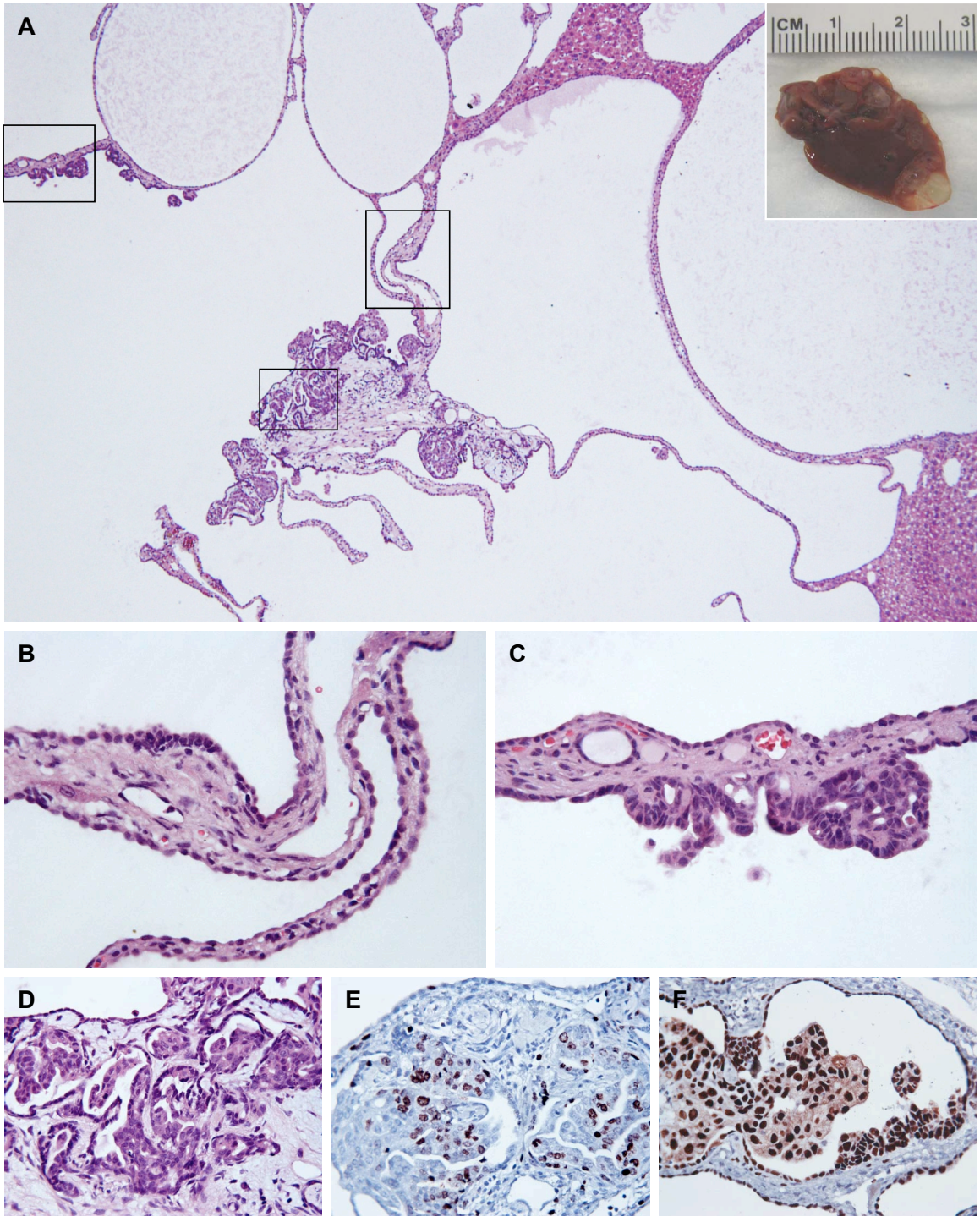

Supplemental Figure 1 NICD-induced cholangiocarcinogenesis. (**A-D**) H&E staining of a large multicystic cholangiocellular tumor detected 20 weeks after plasmid injection (**A**). The inset shows multiple cysts on the surface of the liver in which the tumor formed. Higher magnifications of boxed areas show examples of cystic structures containing flat

or cuboidal cytologically benign cells (**B**), noninvasive cystadenocarcinoma with papillary proliferation of atypical cells (**C**), and invasive cystadenocarcinoma (**D**). (**E** and **F**) Immunostainings (brown) show Ki67 expression predominantly in malignant cells (**E**), and Myc tag expression in all tumor cells (**F**). Original magnification, x40 (**A**); x400 (**B**-**F**).

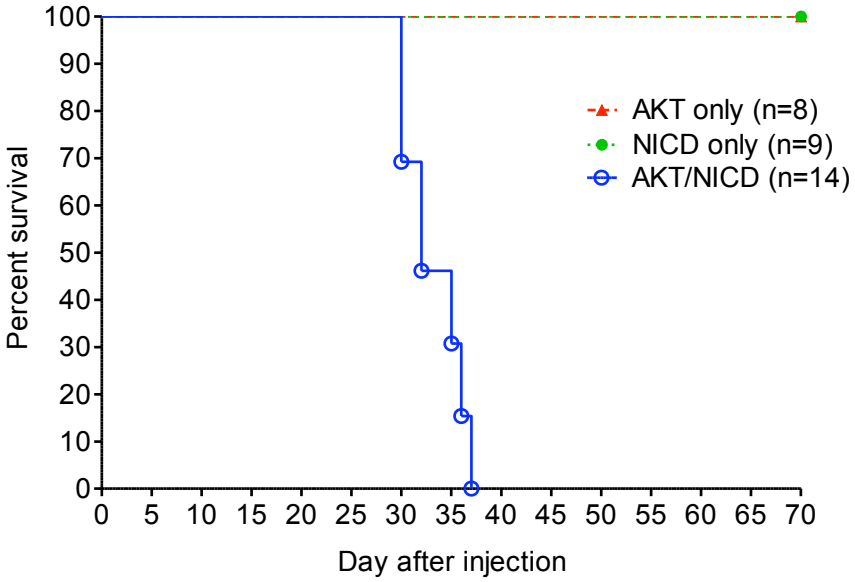

Supplemental Figure 2 Survival curves. Survival of mice injected with NICD, AKT or NICD/AKT plasmids. The number (n) of mice in each group is indicated.

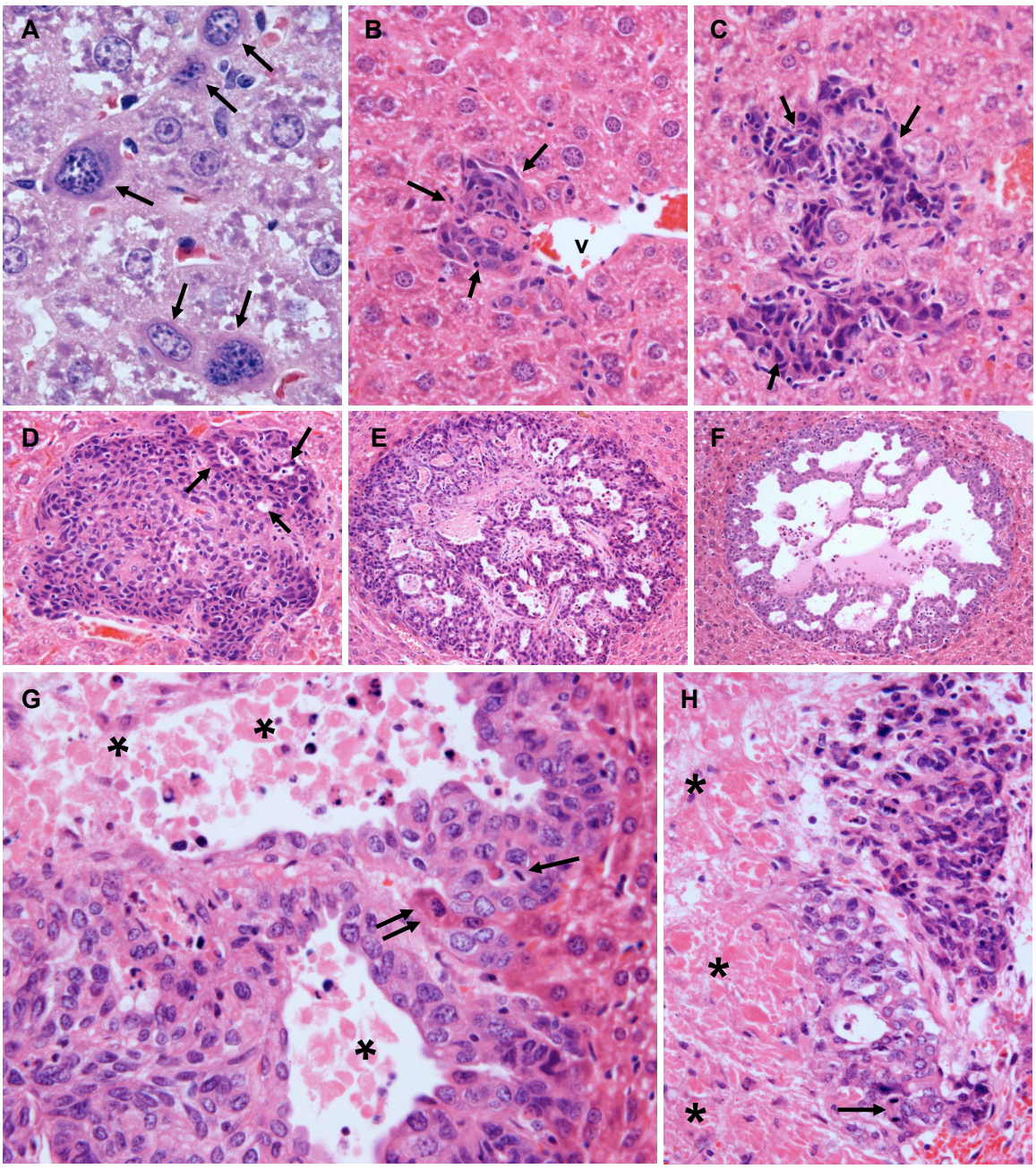

Supplemental Figure 3 Histopathological analysis of NICD/AKT-induced ICC formation. (**A**) Single transformed hepatocytes (arrows) with basophilic cytoplasm and atypical nuclear morphology, including irregular shape, deep infoldings and coarse chromatin, 1.5 weeks after plasmid injection. (**B**) Group of small tumor cells (arrows) with enlarged nuclei next to a hepatic vein (v) 1.5 weeks after plasmid injection. Early ductular structures (**C**, arrows) or glands (**D**, arrows) in small or large tumor 2.5 weeks

after injection. Tumors with typical ductular (**E**) or cystic (**F**) phenotype 3.5 weeks after injection. (**G**) Mitotic figures (arrow), necrotic areas (asterisks) and invasion of the liver parenchyma (enclosed hepatocyte, double arrow) in tumor 4.5 weeks after injection. (**H**) Poorly differentiated tumor with solid areas of mitotically active malignant cells (arrow) and extensive necrosis (asterisks) 5 weeks after injection. H&E stainings. Original magnification, x600 (**A**); x400 (**B**, **C**, **G**, and **H**); x200 (**D**); x100 (**E**); x40 (**F**). At least 15 tumors from 3 mice were analyzed for each time point.

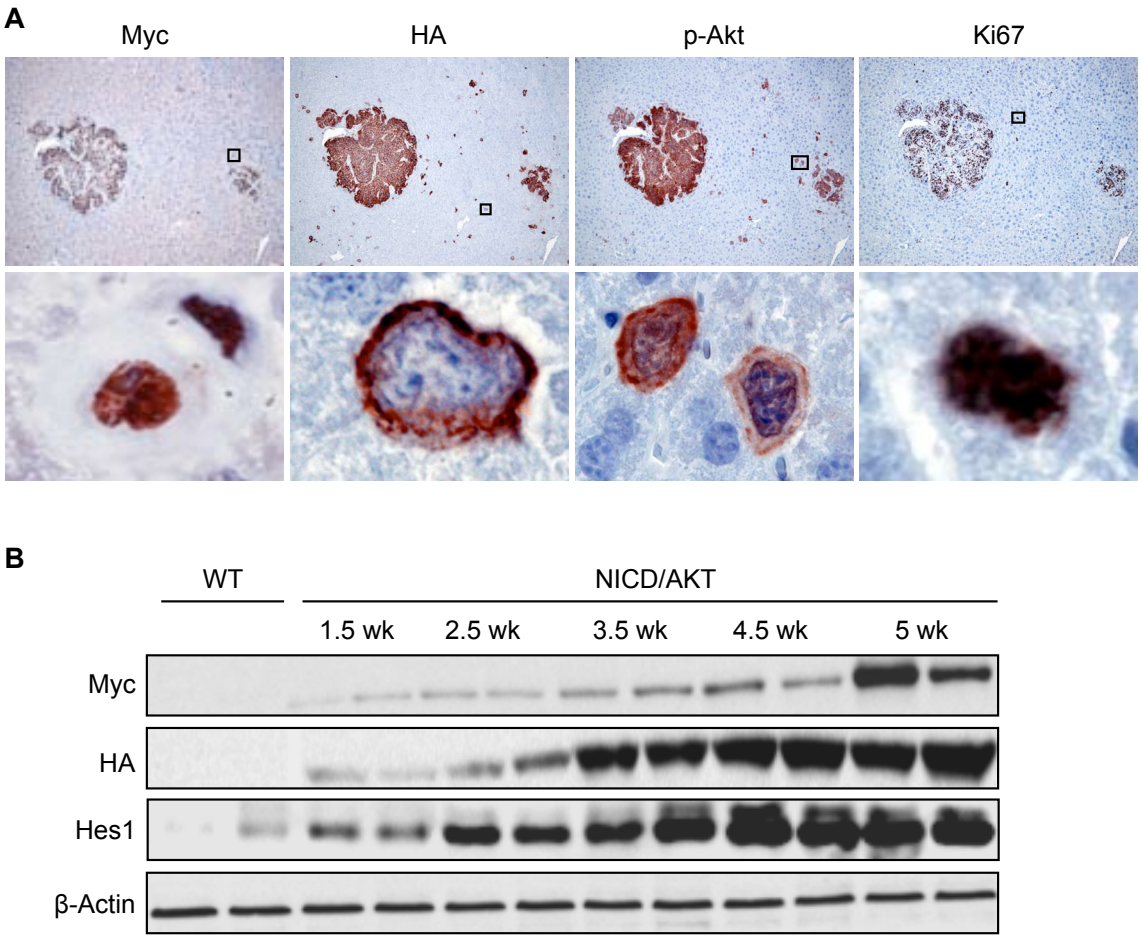

Supplemental Figure 4 Detection of NICD/AKT in ICCs. (**A**) Immunostainings (brown) show expression of NICD Myc tag, AKT HA tag, Akt activated by phosphorylation (p-Akt) and Ki67 in a small and large ICC and single cells. Higher magnifications are shown for single cells in boxed areas. Original magnification, x100 (upper row); x1,000 (lower row). At least 15 liver sections from 3 mice were analyzed for each immunostaining. (**B**) Immunoblotting shows increasing expression of the NICD Myc tag, AKT HA tag and the NICD target Hes1 in NICD/AKT-induced ICCs with time after plasmid injection. β-actin was used as loading control.

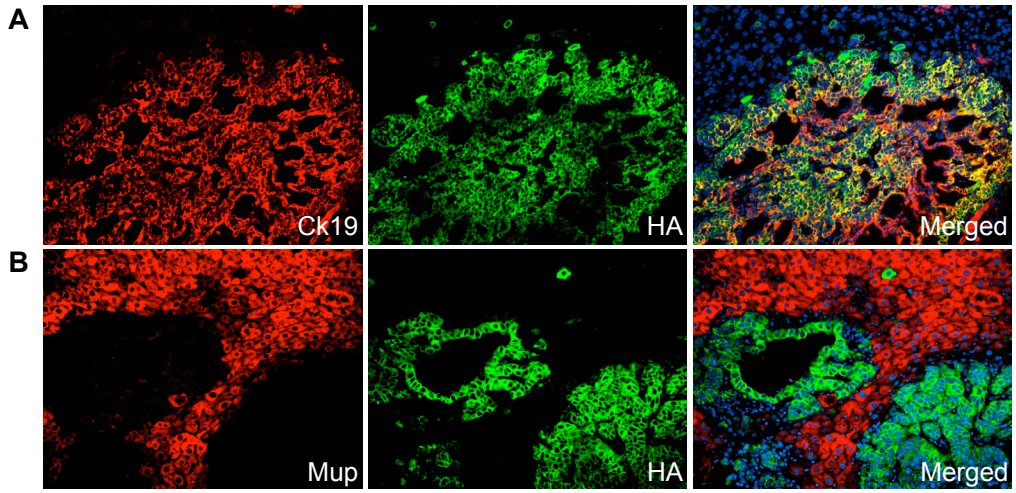

Supplemental Figure 5 Biliary protein expression in NICD/AKT-induced ICCs. (**A**) Coimmunostaining for Ck19 (red) and HA (green) shows biliary differentiation of ICCs. (**B**) Coimmunostaining for Mup (red) and HA (green) shows that ICCs lack hepatocyte differentiation. Original magnification, x200. At least 15 liver sections from 3 mice were analyzed for each immunostaining.

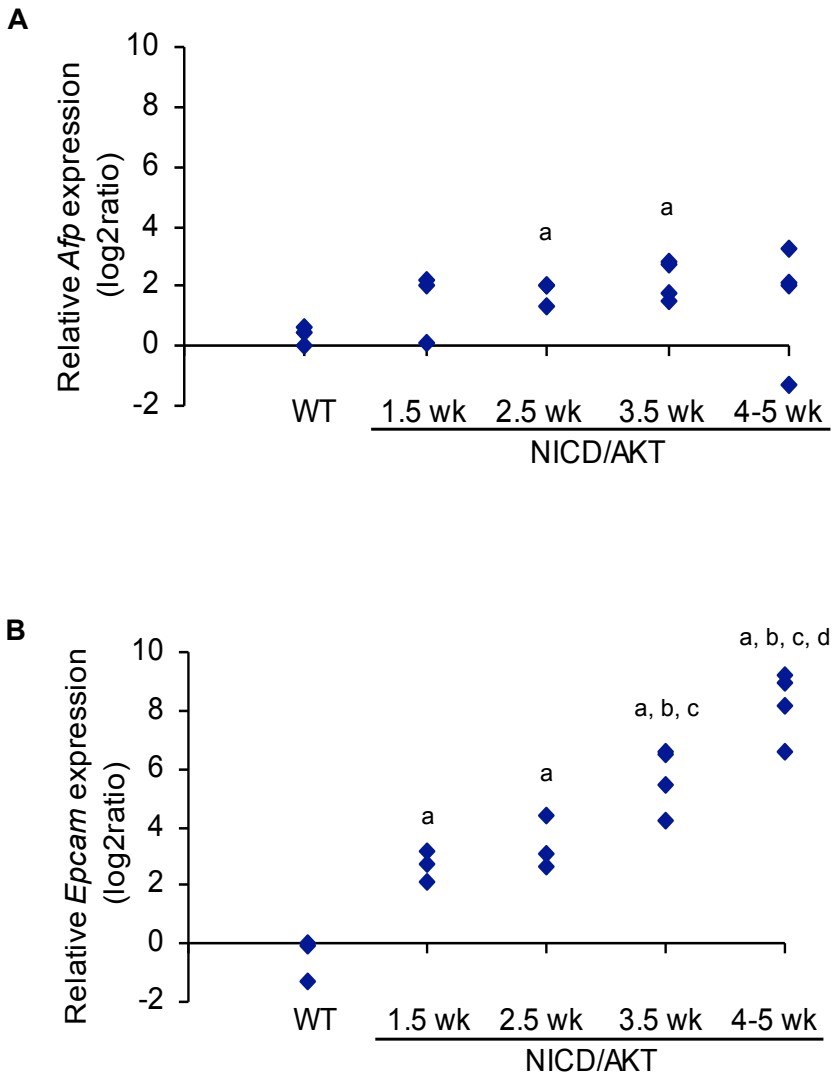

Supplemental Figure 6 Biliary gene expression in NICD/AKT-induced ICCs. (**A** and **B**) qRT-PCR analysis of *Afp* (**A**) and *Epcam* (**B**) gene expression in wildtype livers (WT) and ICCs at different time points after plasmid injection shows a moderate increase in *Afp* and a marked increase in *Epcam* expression. At least 3 mice were analyzed per time point. $P < 0.05$, a: vs WT (control), b: vs NICD/AKT 1.5 weeks, c: vs NICD/AKT 2.5 weeks, d: vs NICD/AKT 3.5 weeks.

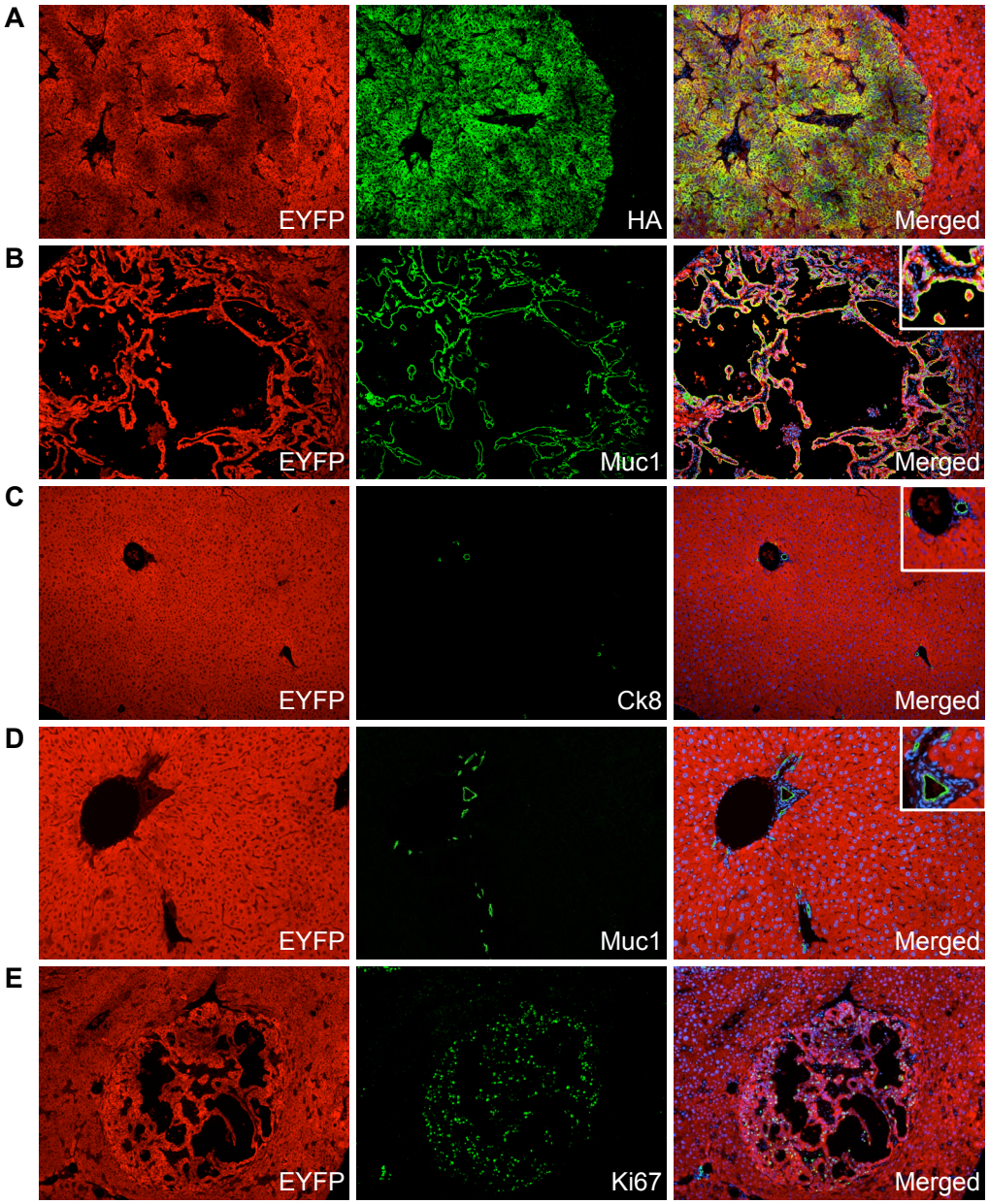

Supplemental Figure 7 Additional analyses and controls establishing the hepatocyte origin of NICD/AKT-induced ICCs. (**A**) Coimmunostaining of tumors for EYFP (red) and HA (green) shows that they originated from hepatocytes in which AKT was stably overexpressed. (**B**) Coimmunostaining of tumors for EYFP (red) and Muc1 (green) shows intense, non-polarized Muc1 expression in ICC cells. (**C**) Coimmunostaining of normal mouse livers for EYFP (red) and Ck8 (green) shows Ck8 expression specifically in BECs. (**D**) Coimmunostaining of normal livers for EYFP (red) and Muc1 (green)

shows localization of Muc1 specifically in the apical membrane of BECs. (**E**) Coimmunostaining of tumors for EYFP (red) and Ki67 (green) shows many proliferating tumor cells. Nuclei were stained with DAPI (blue). Original magnification, x100, insets x200. At least 15 liver sections from 3 mice were analyzed for each immunostaining.

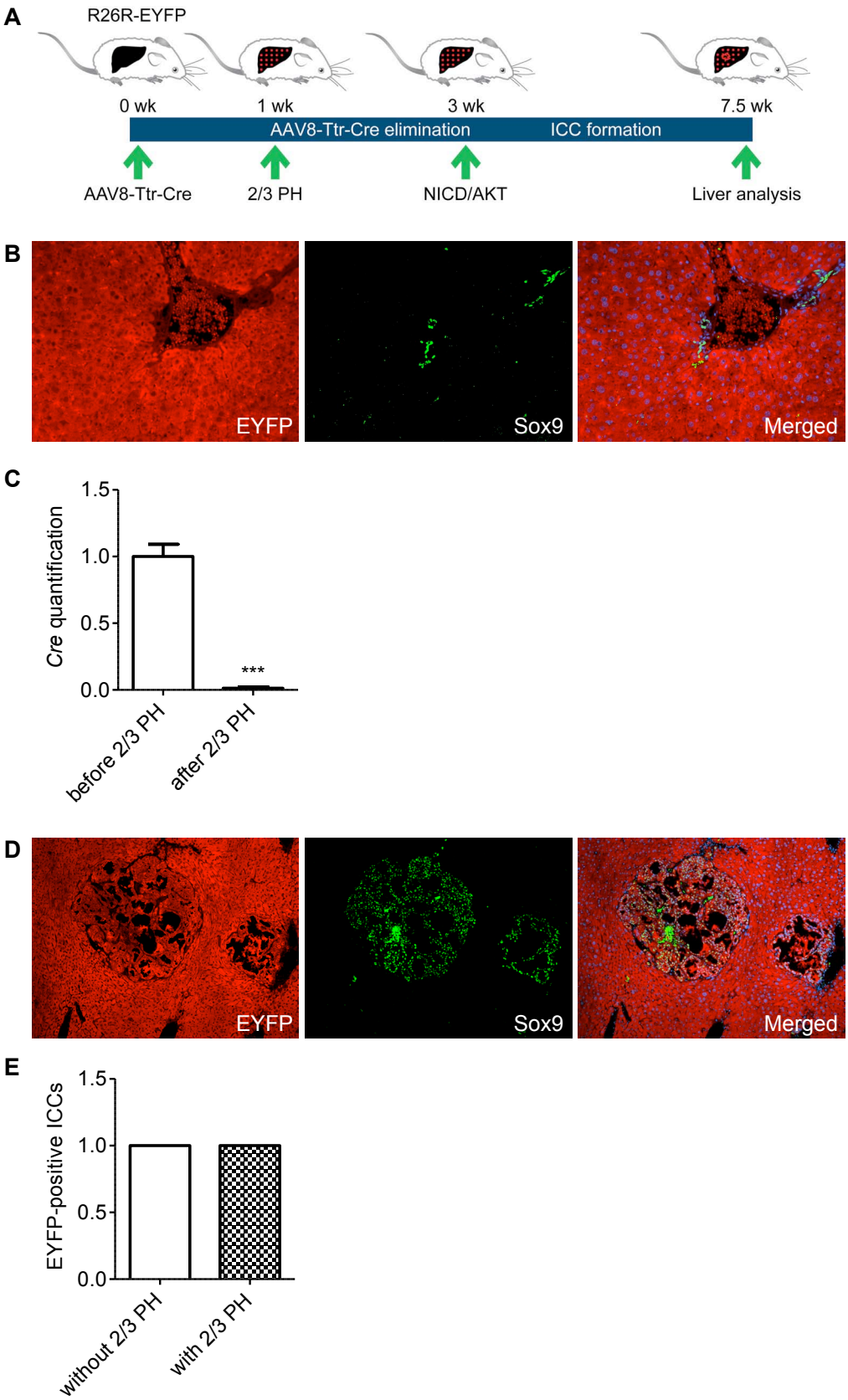
A
R26R-EYFP
0 wk
1 wk
3 wk
7.5 wk
AAV8-Ttr-Cre elimination
ICC formation
AAV8-Ttr-Cre
2/3 PH
NICD/AKT
Liver analysis
B
EYFP
Sox9
Merged
C
Cre quantification
1.5
1.0
0.5
0.0
***
before 2/3 PH
after 2/3 PH
D
EYFP
Sox9
Merged
E
EYFP-positive ICCs
1.5
1.0
0.5
0.0
without 2/3 PH
with 2/3 PH

Supplemental Figure 8 Exclusion of BECs and LPCs as the origin of NICD/AKT-induced ICCs. (**A**) R26R-EYFP mice were intravenously injected with 4 x 10^{11} viral genomes of AAV8-Ttr-Cre, and underwent 2/3 partial hepatectomy (2/3 PH) 1 week later and hydrodynamic tail-vein injection of the NICD/AKT plasmids 3 weeks later. (**B**) Coimmunostaining for EYFP (red) and Sox9 (green) 1 week after AAV8-Ttr-Cre injection shows that all hepatocytes, but not BECs and LPCs, express EYFP. (**C**) Quantitative PCR for *Cre* shows elimination of AAV8-Ttr-Cre from the liver after 2/3 PH. (**D** and **E**) Quantitative analysis of ICCs in EYFP (red) and Sox9 (green) coimmunostainings shows that ICCs are EYFP positive regardless of whether they formed in the presence (without 2/3 PH) or absence (with 2/3 PH) of AAV8-Ttr-Cre, which rules out aberrant expression of AAV8-Ttr-Cre in BECs or LPCs during malignant transformation as the reason for EYFP marker activation in ICCs. Nuclei were stained with DAPI (blue). Original magnification, x100. At least 15 liver sections from 3 mice were analyzed for each time point. Data represent mean ± SEM. ***$P < 0.001$.

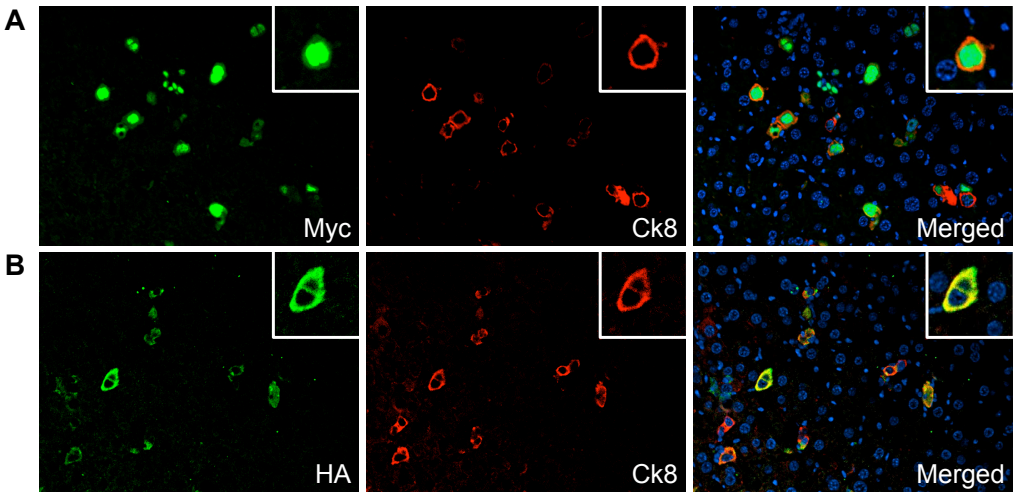

Supplemental Figure 9 Biliary marker expression in single cells expressing NICD/AKT. (**A**) Coimmunostaining for Myc (green) and Ck8 (red) 1.5 weeks after NICD/AKT plasmid injection shows that most cells in the liver parenchyma that express Myc also express Ck8. (**B**) Coimmunostaining for HA (red) and Ck8 (green) confirms this result. Original magnification, x200, insets x400. At least 15 liver sections from 3 mice were analyzed for each immunostaining.

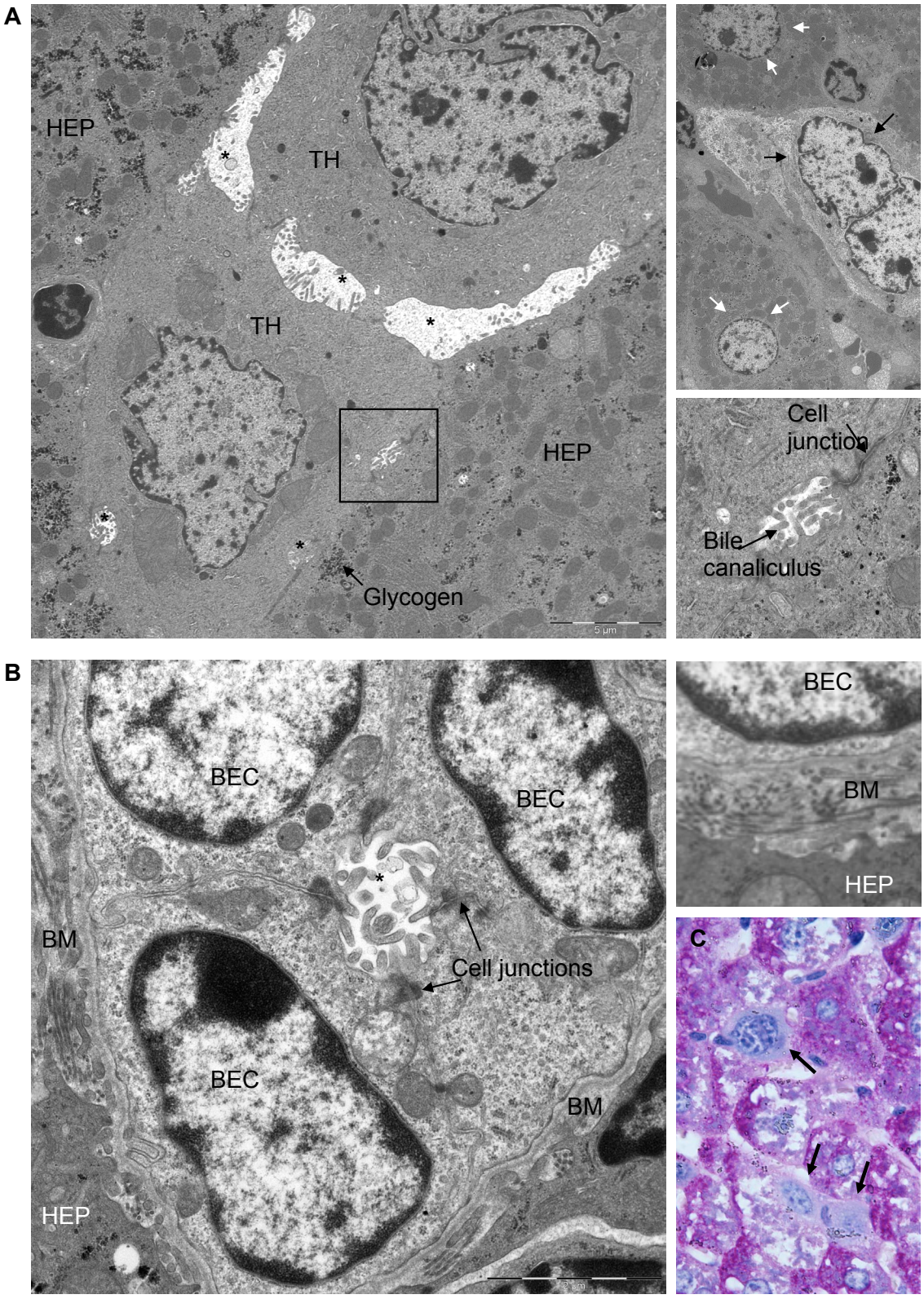

Supplemental Figure 10 Ultrastructural analysis of hepatocytes undergoing conversion

into biliary cells. (**A**) Transforming hepatocytes (THs) form bile canaliculi between each other (asterisks) and with adjacent normal hepatocytes (HEPs; boxed area) 1.5 weeks after NICD/AKT plasmid injection. The bile canaliculi between THs appear primitive. THs show loss of glycogen and nuclear infoldings, as is evident from comparison to nuclei of HEPs shown in a separate image of lower magnification (TH, black arrows; HEPs, white arrows). THs still exhibit cell junctions with HEPs, as shown in the higher magnification of the boxed area. (**B**) Normal biliary epithelial cells (BECs) forming a small bile duct (asterisk) exhibit cell junctions with each other, but not with adjacent HEPs. BECs are separated from HEPs by a collagenous basement membrane (BM), as shown in the higher magnification image. (**C**) Example of PAS staining used to identify THs (arrows) for electron microscopy. Original magnification, x600.

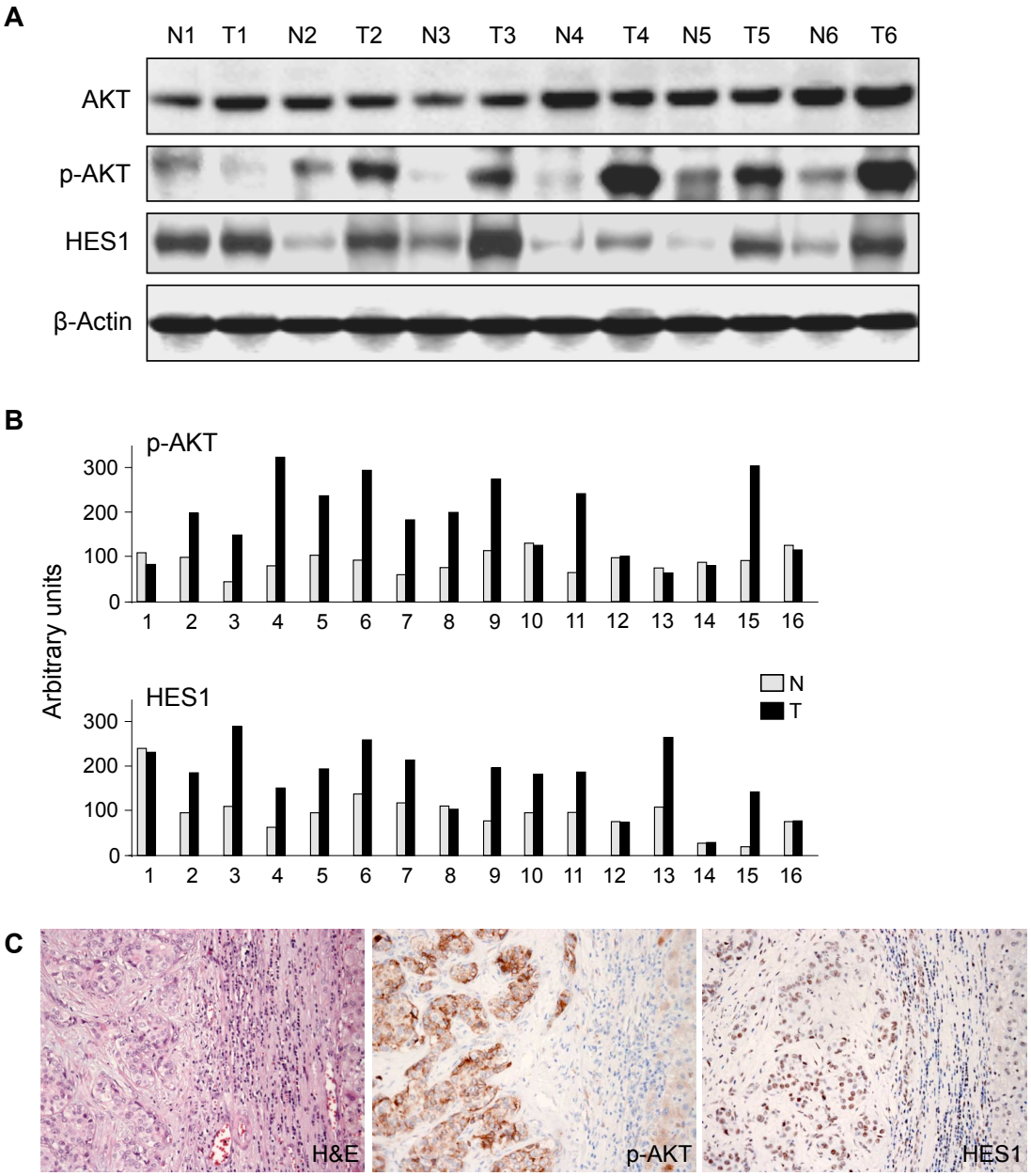

Supplemental Figure 11 Activation of AKT and NOTCH signaling in human ICCs. Analysis of p-AKT and HES1 expression in 16 human ICCs (T) and respective surrounding normal liver (N). (**A**) Total AKT, p-AKT and HES1 immunoblottings of T/N1-6 are shown as representative examples. (**B**) Quantification of signal intensities of p-AKT and HES1 immunoblottings of all T/N pairs. (**C**) H&E staining and immunostainings (brown) for p-AKT or HES1 of serial sections of T/N4. Many more

cells in the tumor are positive for p-AKT and HES1 than in the surrounding normal liver. Original magnification, x200.

Supplemental Table 1 Primary Antibodies

Antigen	Species	Dilution	Supplier
AKT	Rabbit	1/100	Cell Signaling
p-AKT (Ser473)	Rabbit	1/100	Cell Signaling
Ck8	Rat	1/100	DSHB
Ck19	Rabbit	1/100	Abbomax
Ck19	Rat	1/50	DSHB
GFP	Chicken	1/200	Abcam
HA	Mouse	1/2000	Cell Signaling
HA	Rabbit	1/100	Santa Cruz
Hes1	Rabbit	1/100	Abcam
Ki67	Rabbit	1/100	Thermo Scientific
Muc1	Hamster	1/100	Thermo Scientific
Mup	Goat	1/200	Cedarlane
Myc	Mouse	1/200	Invitrogen
Myc	Mouse	1/200	Cell Signaling
Sox9	Rabbit	1/75	Millipore

Supplemental Table 2 Secondary Antibodies

Reactivity	Species	Fluorochrome	Dilution	Supplier
Chicken	Donkey	DyLight 549	1/200	Jackson Immunoresearch
Goat	Donkey	Alexa Fluor 488	1/200	Molecular Probes
Hamster	Goat	DyLight 488	1/100	Jackson Immunoresearch
Mouse	Rabbit	HRP	1/100	BD
Rabbit	Donkey	DyLight 488	1/200	Jackson Immunoresearch
Rabbit	Donkey	DyLight 649	1/100	Millipore
Rat	Donkey	DyLight 488	1/200	Jackson Immunoresearch